ESA Climate Change Initiative
aerosol_cci+

Algorithm Theoretical Basis Document (ATBD)
Instruments: ATSR-2 and AATSR
Algorithm: SU-ATSR

Version 4.35

DOCUMENT STATUS SHEET

	FUNCTION	NAME	DATE	SIGNATURE
LEAD AUTHOR	editor	Peter North	04/5/2021	
CONTRIBUTING AUTHORS	Algorithm development	Andreas Heckel	22/3/2021	
	Algorithm development	Kevin Pearson	22/3/2021	
REVIEWED BY	Co-science leader			
APPROVED BY	Technical officer (ESA)			
ISSUED BY	Project manager			

EXECUTIVE SUMMARY

The SU-ATSR algorithm has been developed at Swansea University for estimation of atmospheric aerosol and surface reflectance for the ATSR-2 and AATSR sensors. Over land, the algorithm employs a parameterised model of the surface angular anisotropy, and uses the dual-view capability of the instrument to allow estimation without a priori assumptions on surface spectral reflectance. Over ocean, the algorithm uses a simple model to exploit the low ocean leaving radiance at red and infra-red channels at both nadir and along-track view angles. While previous versions of the algorithm have been described in depth in previous publications, a number of innovations are documented here developed under the aerosol CCI project. Developments under the Aerosol CCI programme include (i) enhanced treatment of aerosol mixtures, (ii) inclusion of a model of ocean surface including wind-speed and pigment dependency, and (iii) analytical propagation of uncertainty. This ATBD summarises the underlying principles, equations input/output and implementation details of the algorithm, based on the algorithm version 4.35.

Issue	Date	Modified Items / Reason for Change
1.0	4/3/2011	First edition
2.0	10/9/12	Major revision, to document developments under the Aerosol CCI project: Section 4.1 Surface treatment. New ocean model based on Aerosol_cci recommendations Section 5.1 Cloud screening and preprocessing. Options added to use alternative cloud masks. Section 5.2: Aerosol model and climatology. Upgraded algorithm now uses common aerosol model set, and allows continuous variation of aerosol properties based on mixtures of these, and use of climatology of composition as a prior. Section 8: Error budget estimates. New analytic error propagation equations.
3.0	15/6/2017	Revision to reflect changes up to current version SU 4.3, which concern refinements to operational implementation (section 5) Section 5.1 new section with added development and detail on super-pixel aggregation Section 5.3 Aerosol climatology added explaining definition and use of aerosol climatology in inversion Section 5.5 Inversion procedure modified and expanded to include detail on constraints on the inversion, including introduction of 'smoothness' constraint between super-pixels Section 5.6 added detailing post-processing for cloud contamination reduction
4.0	22/03/2021	Compatible version with dataset and code version 4.33. ATBD changed structurally throughout to improve clarity and compatibility with SLSTR version.
5.0	31/03/2022	Compatible version with dataset and code version 4.35. ATBD changed to include additional spectral constraint.

LIST OF TABLES

LIST OF FIGURES

TABLE OF CONTENTS

1 INTRODUCTION

This document describes the theoretical basis for the aerosol retrieval algorithm developed for ATSR-2 and AATSR by Swansea University This algorithm is referred to as SU-ATSR, with current version v4.35. The SU-ATSR algorithm has been extensively described in a series of peer-reviewed papers [references listed by number in section 1.2.2] and reports [references listed by number in section 1.2.2]. This ATBD aims to provide an overview of the algorithm with detailed references to the above-mentioned papers and reports, with summaries of the issues that are important for the aerosol-cci work, and developments to the algorithm made within the CCI project.

1.1 References

1.1.1 Applicable Documents

[AD1]   The Statement of Work, reference ESA-CCI-EOPS-PRGM-SOW-18-018, issue 1, revision 6, dated May 31st, 2018, and its specific annex C.

[AD2]   The Contractor's Proposal reference 3022091 revision 1.1 , dated 10 December 2018

1.1.2 Reference Documents

[RD1]   Bevan, S.L., North, P.R.J., Grey, W.M.F., Los, S.O. and Plummer, S.E. (2009), Impact of atmospheric aerosol from biomass burning on Amazon dry-season drought. Journal of Geophysical Research, **114**, D09204, doi:10.1029/2008JD011112.

[RD2]   Bevan, S.L., North, P.R.J., Los, S.O. and Grey, W.M.F. (2012). A global dataset of atmospheric aerosol optical depth and surface reflectance from AATSR. Remote Sensing of Environment, 116, 119-210.

[RD3]   Davies, W.H., North, P.R.J., Grey, W.M.F. and Barnsley, M.J. (2010), Improvements in Aerosol Optical Depth Estimation using Multi-angle CHRIS/PROBA Images, *IEEE Transactions on Geoscience and Remote Sensing,* **48**(1), 18-24.

[RD4]   Grey., W.M.F., North., P.R.J., Los, S.O., and Mitchell, R.M., (2006). Aerosol optical depth and land surface reflectance from multi-angle AATSR measurements: Global validation and inter-sensor comparisons. *IEEE Transactions on Geoscience and Remote Sensing, 44(8)*, 2184 – 2197.

[RD5]   Grey., W.M.F, North., P.R.J., and Los, S. (2006b). Computationally efficient method for retrieving aerosol optical depth from ATSR-2 and AATSR data, *App. Optics*, **45(12):** 2786-2795.

[RD6]   North, P.R.J., Briggs, S.A., Plummer, S.E. and Settle, J.J., (1999). Retrieval of land surface bidirectional reflectance and aerosol opacity from ATSR-2 multi-angle imagery, *IEEE Transactions on Geoscience and Remote Sensing*, **37(1),** 526-537.

[RD7]   North, P. R. J. (2002). Estimation of aerosol opacity and land surface bidirectional reflectance from ATSR-2 dual-angle imagery: Operational method and validation, *J. Geophys. Res*., **107**, doi:10.1029/2000JD000,207.

[RD8]   North, P.R.J., Brockmann , C., Fischer, J., Gomez-Chova, L., Grey, W., Heckel, A., Moreno, J., Preusker, R. and Regner, P. (2008). MERIS/AATSR synergy algorithms for cloud screening, aerosol retrieval and atmospheric correction*. In Proc. 2nd MERIS/AATSR User Workshop, ESRIN, Frascati, 22- 26 September 2008.* (CD-ROM), ESA SP-666, ESA Publications Division, European Space Agency, Noordwijk, The Netherlands.

[RD9]   *ESA Climate Change Initiative Aerosol_cci, Technical note: Aerosol models*. Version 1.1, G. de Leeuw (Ed)., 2011.

2 INSTRUMENT CHARACTERISTICS

The ATSR-2 instrument was hosted on the ERS-2 satellite, and provides a record from 1995-2003, and succeeded by the AATSR instrument hosted on ENVISAT, for the period 2002-2012. The AATSR instrument is a scanning radiometer, sensing at thermal infrared, reflected infra-red and visible wavelengths with two ~500 km wide conical swaths, with 555 pixels across the nadir swath and 371 pixels across the forward swath. The specifications of AATSR and ATSR-2 are the same, except that the ATSR-2 instrument employed a reduced swath of visible channels over and near oceans due to data transmission restrictions. The set of channels are listed in Table 1. The nominal pixel size is 1 km^2 at the center of the nadir swath and 1.5 km^2 at the center of the forward swath. For the AATSR level 1 products the forward pixels are sampled to 1km in order to be the same size as the nadir pixels. The conical scan provides two views of the surface and improves the capacity for atmospheric correction and enables observations of the ocean surface under a solar zenith angle of ~55° in the forward direction. The channels at 1.6μm and 0.87μm are especially important to correct for the impact of aerosols, especially above coastal waters, since at this spectral range there is nearly no backscattering of solar radiation emanating from the water body. For land aerosol retrieval, the bands at shorter wavelengths (550nm and 665nm) where aerosol scattering is greater with respect to surface scattering are important.

Table 1: AATSR and ATSR-2 spectral channels

Channel	Wave-length (nm)	Band-width (nm)
1	550	20
2	665	20
3	865	20
4	1610	60
5	3740	380
6	10850	90
7	12000	1000

3   ALGORITHM

Here we introduce the background and motivation to the algorithm, which exploits the ATSR dual angle for retrieval of aerosol optical thickness and type over both land and ocean.

3.1   Theoretical background

Atmospheric aerosols also represent one of the greatest uncertainties in our understanding of the climate system (Solomon et al., 2007; Bellouin et al., 2005; IPCC 2013). This is principally due to a lack of accurate and repetitive measurements at global scales, in particular over the land surface where it is difficult to separate surface scattering from the atmospheric signal. Aerosols influence climate change through their direct radiative forcing and link with cloud formation, their influence on the directionality of the surface downwelling radiation and their possible feedbacks with rainfall (Twomey 1974; Rosenfeld et al., 2001; Bevan et al., 2009). In addition, the high spatial and temporal variability of aerosol scattering typically represents the greatest uncertainty in derivation of surface reflectance over land, needed for estimation of surface albedo and change detection over time. The parameters required to model aerosol radiative effects are AOD for a given reference wavelength, and aerosol model, describing spectral dependence of AOD, single scattering albedo, and phase function. Reviews of satellite aerosol retrieval methods and comparisons within the ESA Aerosol Climate Change Initiative are given in Holzer-Popp et al. (2013), de Leeuw et al. (2015) and Popp et al. (2016). Here we outline the main approaches to aerosol retrieval relevant to polar orbit optical instruments such as the ATSR series.

3.1.1   Aerosol optical thickness and scattering properties

The parameters required to model aerosol radiative effects are aerosol optical depth (AOD) for a given reference wavelength, and spectral dependence of optical depth, single scattering albedo, and phase function. These properties are closely related to aerosol amount, composition and size distribution. The net effect of aerosol on climate forcing depends on its optical properties (absorption and scattering) (Mishchenko et al., 2007). Currently, atmospheric radiative transfer (RT) codes allow retrieval of surface reflectance with a high degree of precision for a known atmospheric profile, with theoretical error typically <0.01 in surface reflectance (Fischer and Grassl, 1984; Kotchenova et al., 2006). This enables both forward simulation of satellite radiances, and inversion of such models to estimate surface reflectance given a set of top-of-atmosphere (TOA) radiances. To date, most retrieval schemes return spatially varying estimates of AOD as the main parameter, and some additionally return information on aerosol size distribution (e.g. Remer et al., 2005) or the related property of Angstrom coefficient (e.g. Veefkind et al 1999). Recent methods have explored search for the most probable candidate aerosol model from a limited database, based on fit to the observations, with further aerosol properties defined by this model (North 2002b; Holzer-Popp et al., 2008; Diner et al., 2009; Bevan et al., 2012).

3.1.2 Satellite retrieval methods

3.1.2.1 Single-view methods

Most currently available aerosol retrievals are based on data from instruments with a single sampling of the angular domain. These algorithms are based on different assumptions, depending on available spectral sampling. In general, the retrievals need to use known wavelength dependence of surface reflectance in order to provide information on the aerosol. In general, it is more challenging to retrieve required aerosol properties over the land than the ocean. This is because the scattering from the land surface tends to dominate the satellite signal making it difficult to discern the atmospheric scattering contribution, particularly over bright surfaces. In addition, obtaining an accurate model of the land surface is further complicated because bi-directional reflectance is highly variable, both spatially and temporally.

The separation of the surface contribution is always based on a priori knowledge about the spectral properties of the surface. A number of assumptions have proven successful:

- Identification of dark targets: where it is possible to identify targets of dark dense vegetation (DDV) with known spectral properties, this may be used to derive aerosol path radiance over these targets (Kaufman and Sendra (1988)). Operational algorithms have been developed for MODIS (Remer et al., 2005; Levy et al., 2015), and MERIS (Santer et al., 1999; Santer et al., 2007) on this basis, amongst other instruments. For MERIS, the vegetation index ARVI (Kaufman et al., 1992) is used to identify vegetation. However, accurate application is limited to regions where such targets are available at the appropriate spatial resolution (i.e. oceans and dark dense vegetation), so we must employ interpolation of the aerosol field to derive values at image points suitable for atmospheric correction. Improvement of this method is possible using calibration of the spectral relationship over a range of representative land covers, corresponding to selected AERONET sites (Levy et al., 2007) allowing correction for view-angle effects on surface spectra and generalisation to brighter surfaces (Hsu et al., 2004, Hsu et al., 2013).

- Spectral mixing: Independently measured spectra of vegetation and bare soil are taken to construct a basis and the actual surface spectrum is assumed to be a linear combination of both, depending on vegetation cover. The algorithm described by von Hoyningen-Huene et al. (2003), bases the mixture of soil and vegetation spectra on the measured NDVI. The thus defined surface spectrum is then only allowed for scaling. An alternate algorithm developed by Guanter et al. (2007) uses mainly the assumption that aerosol is spatially more homogeneous than surface reflectance. Therefore the algorithm searches locally for pixels with the most and the least vegetation cover (darkest and brightest pixels) and assumes the atmospheric information to be constant. This allows the determination of the aerosol content. The MERIS AATSR/SYNERGY retrieval and corresponding SYN branch for OLCI and SLSTR uses a spectral mixing constraint in addition to multi-angular information to improve aerosol and surface reflectance retrieval

- *A priori* assumptions based on existence of an independent estimate of surface

reflectance from other instruments: For example Thomas et al. (2009) used MODIS estimates of surface reflectance to estimate aerosol from (A)ATSR instruments. While potentially allowing spatially continuous mapping of aerosol, important limitations are the reliance on the existence of a recent reflectance map from another instrument which has already been successfully corrected for atmospheric scattering, as well as including errors due to different temporal, angular and spectral sampling.

While potentially offering accurate retrieval where the target reflectance matches well with modelled spectrum, a single spectral measurement can give information on aerosol path radiance only, and not on phase function. Generally these methods, are suitable only for dark targets with relatively low spectral variability, so give a sparse estimate of optical depth, and are normally inappropriate for bright surfaces such as arid or snow-covered land

3.1.2.2 Multi-temporal methods

Related to single view retrieval methods are those which allow retrieval from time series, assuming greater stability of land surface reflectance compared to aerosol (Lyapustin, A. and Wang 2009; Hsu et al., 2013). The time series allows use of recent reflectance retrievals as a prior in inversion. Such techniques are particularly relevant where high temporal sampling is available, such as from geostationary instruments, for example the method by Govaerts et al., (2010) using optimal estimation theory and including a model of the effects of solar angle change on land surface scattering.

3.1.2.3 Multiple view-angle (MVA) methods

While spectral methods may produce very good results in regions where the assumptions are fulfilled, global aerosol retrievals show a number of uncertainties due to the large variability in spectral surface properties. Use of multiple view-angle imagery allows an additional constraint to be placed, since the same area of surface is viewed through different atmospheric path lengths. The concept was pioneered by ATSR on ERS-2, originally for atmospheric correction of SST for the effects of water vapour (Barton et al., 1989). In addition, there is scope to use the increased angular sampling of the land surface to further constrain retrieval of albedo and vegetation biophysical parameters (Diner et al., 1999). Several instruments have been designed to exploit the ability of MVA techniques for aerosol retrieval, including MISR, using 9 cameras tilted at angles in the range ± 70.5° along-track, and POLDER, which employs a CCD array to sample continuousl9 at ± 43° along-track (Martonchik et al., 1998; Leroy et al., 1997).

For the ATSR instrument series, 2 view directions are available, at approximately nadir and 55° along-track requires an approach which exploits the similarity of the surface anisotropy across wavelengths. This is due to the fact the anisotropy is dominated by geometric shadowing effects, which are wavelength invariant. However other effects contribute to anisotropy; the differential viewing of canopy/understory surfaces with view angle, and the degree of multiple scattering, which tends to reduce anisotropy over bright surfaces. A simple approximation assuming spectral invariance of the BRDF (Mackay et al., 1999; Flowerdew and Haigh, 1996). has been used in inversion schemes (Veefkind et al., 2000) to provide a successful retrieval of aerosol. The method has developed further to include enhanced modelling of the spectral variation of anisotropy (North et al., 1999) to give an operational method from which global retrieval of aerosol properties has been achieved using the ESA Grid Processing on Demand

(GPOD) system (North 2002b; Grey et al., 2006a,b). Validation by comparison with AERONET shows robust retrieval over all land surfaces, including deserts (Grey et al., 2006b; Bevan et al., 2009). The method has also recently been applied to estimation of aerosol from the CHRIS PROBA instrument, by exploiting the ability of the instrument to acquire 5 views of the target by satellite pointing, and used for simulation of Sentinel-3 spectral and viewing geometry (Davies et al., 2010; Davies et al., 2015). The use of a cross-spectral constraint on surface anisotropy has also recently been incorporated into the MSR processing algorithm (Diner et al., 2005).

The principal advantage of an MVA approach is that no *a priori* information of the surface spectrum is required and aerosol properties can be retrieved over all surface types, including bright deserts. Limitations of the angular approach are that the algorithms require accurate co-registration of the images acquired from multiple view angles. Normally aerosol is retrieved at a lower resolution than the pixel resolution, to decrease the effect of misregistration errors, for example at 18km for MISR and 9km for ATSR (Diner et al., 2009; North et al., 2002b), and the methods may be sensitive to undetected sub-pixel clouds (North et al., 1999). Algorithms using dual view AATSR were further developed under the ESA Aerosol Climate Change and independent evaluation recommended the retrieval based on the Swansea University algorithm (SU-AATSR) to form the first CCI full mission (17 year) dataset to be submitted for the OBS4MIPS Initiative (Holzer-Popp et al. (2013), de Leeuw et al. (2015) and Popp et al. (2016)).

3.2   Algorithm outline

The aim is to make use of the angular and spectral sampling available from AATSR and ATSR-2 to allow aerosol retrieval over land and ocean. The method takes as input TOA reflectance data for the 4 solar reflective (A)ATSR bands, at both nadir and oblique views, giving a total of 8 input channels, and information present on solar/view geometry, location, and identification per-pixel of cloud, water, ice/snow. The output is aerosol optical depth at a reference waveband, an estimate of aerosol fine mode fraction, and further derived properties such as absorption and spectral dependence of AOD.

The problem is formulated as one of optimisation subject to multiple constraints, which has been widely applied to atmospheric retrievals (Dubovik 2005). Figure 1 illustrates the retrieval framework followed here. The two-stage optimization process is employed: (1) Given a set of satellite TOA radiances, and an initial guess of atmospheric profile, we estimate the corresponding set of surface reflectances. (2) Testing of this set against a constraint results in an error metric, where a low value of this metric should correspond to a set of surface reflectances (and hence atmospheric profile) which is realistic. Step (1) is repeated with a refined atmospheric profile until convergence at an optimal solution. Two parameters describing the aerosol content are directly retrieved during the inversion: AOD at 550nm (τ_{550}) and fine mode fraction (*FMF*), while further aerosol parameters are constrained by a climatology giving likely seasonal and spatial sources of aerosol. The algorithm components are therefore (i) design of an efficient and accurate scheme for deriving surface reflectance for known atmospheric profile, (ii) formulation of constraints on the land surface reflectance suitable for (A)ATSR, and (iii) iterative inversion scheme to retrieve the free aerosol parameters.
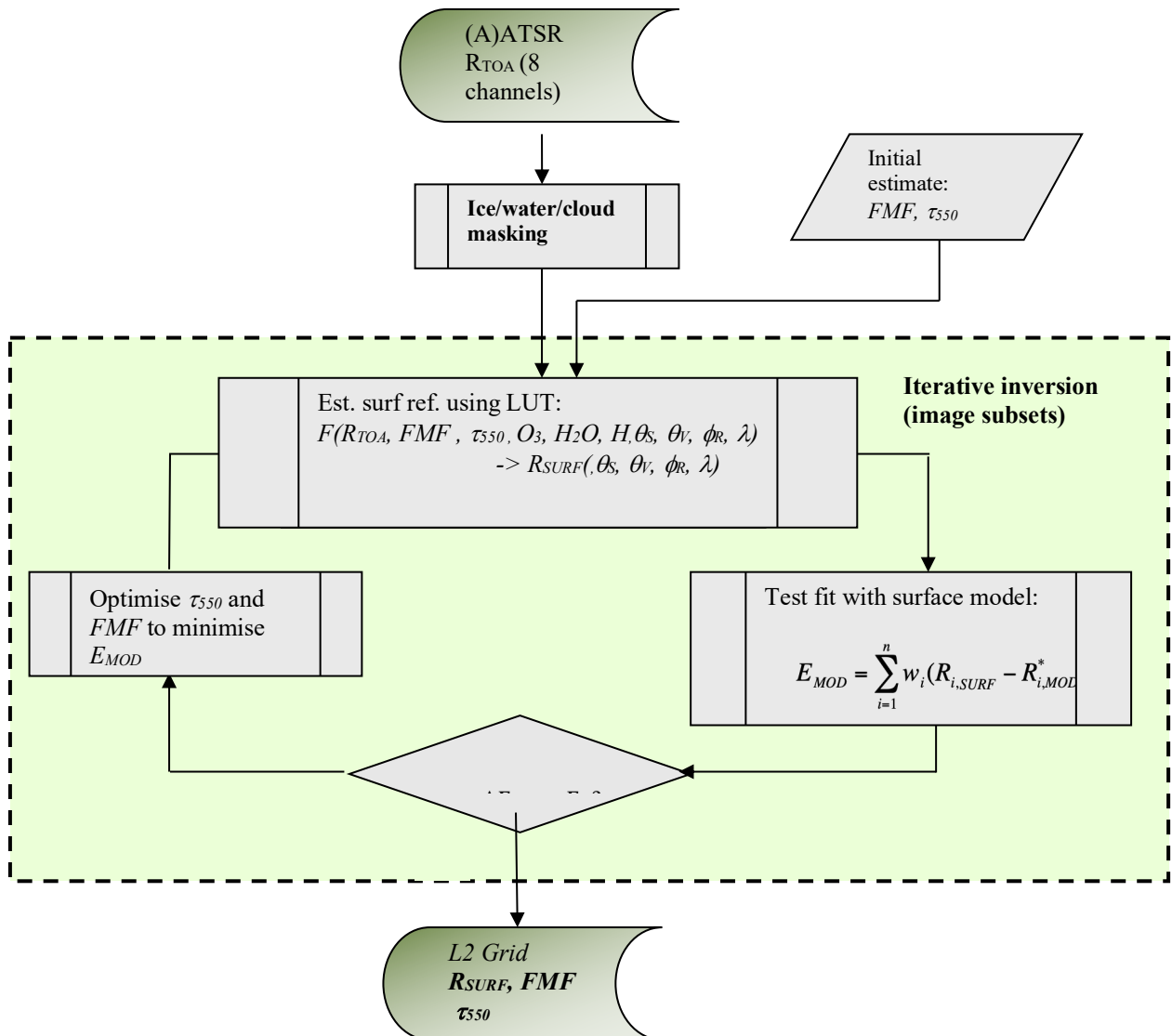
Figure 1 - Outline processing algorithm for retrieval of and aerosol properties (optical depth τ_a and Fine Mode Fraction (FMF)) from AATSR data. The principle is iterative inversion based on fit of derived surface reflectance to a parameterised model of reflectance over land or ocean, R_{MOD}.

3.3 Cloud detection and preprocessing

The algorithm requires screening of input pixels unsuitable for aerosol retrieval, to include cloud, sun glint, snow or ice pixels. It therefore requires a masking or removal of all invalid pixels prior to any further processing. As the aerosol retrieval scheme treats ocean and land pixels differently a separation between valid land and valid ocean pixels needs to take place before subsequently accumulation of the valid pixels into superpixels can be done.

3.3.1 Cloud screening / pixel classification

The surface is also classified into land or ocean to determine the algorithm which should be used. Pixels to exclude from processing should be those flagged as either, snow/ice or glint in the L1b product. In addition all 8 direct neighbours of a cloudy pixel should be considered as potentially cloud contaminated and hence regarded as invalid as well. Pixels are screened independently at nadir and forward views; due to parallax related to cloud height, corresponding pixels will not necessarily be flagged.

The implementation uses the (A)ATSR supplied cloud flags with some additional tests. AATSR v2.1 products processed using Instrument Processing Facility version 6.01 (IPFv6.01) improve on the cloud tests of IPFv6.0 which were optimised for use over ocean (Zavody et al. 2000). The IPF improvements consist of applying a gross cloud test over land based on the 12 μm brightness temperature, disabling the spatial coherence test over land, and applying a test based on normalised difference indices using the visible channels (Birks 2007). The instrument flags set if pixel is free of cloud, ice and glint is referred to as *land_ocean_clear_mask*. To these tests further tests were added based on those described by Plummer (2008), referred to as *apollo_clear_mask*. Separate cloud masks for nadir and forward views are derived. A further test implemented over land, and used in combination with the instrument mask in order to reduce over-flagging of cloud, is to perform a screening of cloud based on histograms brightness, spectrum and temperature histograms based on algorithm developed by FMI (Sogacheva et al., 2017), referred to as *hist_clear_mask*.

The flags are combined as follows:

• Over land, pixel is labelled as clear if *land_ocean_clear_mask OR apollo_clear_mask OR hist _clear_mask*.

• Over ocean, pixel is labelled clear if *land_ocean_clear_mask OR apollo_clear_mask*

Over ocean, for glint an additional test is introduced based on the experience in of algorithm development during the Aerosol CCI project. This additional test makes use of the tabulated values of ocean BRF used for the ocean part of the aerosol retrieval. The LUT is used to estimate the ocean BRF in the 1.61um band for the viewing geometry of a given pixel assuming no AOD and a wind speed of 9m/s. Should the modelled ocean BRF in the 1.6um band exceed a reflectance of a threshold value of 0.008 the pixel is regarded as potentially glint contaminated and declared invalid.

3.3.2 Super-pixel aggregation

Although AATSR radiances are retrieved at a spatial resolution of 1km2, groups of 9 x 9 pixels are averaged before processing in order to reduce noise and minimise errors in coregistration between the forward and nadir images. The fraction of pixels in each 9 x 9 group required to be cloud free and of a given surface type is configurable. In the current version 75%, i.e. 61 of the 81 pixels need to cloud free or processing. The actual number of available pixels per bin is reported by the algorithm and available in the output product.

Parameters such as geo-location, viewing geometry and acquisition time can therefore be directly inferred from the corresponding centre pixel. The geo-position and acquisition time of the super-pixel is defined to be the corresponding time of the nadir pixels. Over land, for each pixel, both nadir and corresponding oblique pixels must be valid to accumulate that pixel within the super pixel aggregate, since the surface reflectance may be spatially homogenous. Over ocean the pixels aggregated to either nadir or oblique may be clear in that view only.

For a super-pixel to be valid the number of valid pixels in the bin needs to be evaluated separately for land and ocean. If more than 50% of either land or ocean pixels are valid the super-pixel can be considered valid for retrieval. The spectral radiance of the super pixel is then represented by the arithmetic mean of the spectral radiances of the valid pixels. As the threshold is 50% a super-pixel can only be processed by either the land or ocean part of the retrieval. For dual view retrievals over land, both corresponding super-pixels need to be valid.

The result is a 'super-pixel' giving aggregated cloud-free TOA radiance for nadir and oblique view (if present) of the same surface location. Over ocean retrieval proceeds if either nadir or oblique super-pixels are valid (i.e. formed from at least 50% of valid pixels), while over land both nadir and oblique must be valid.

3.4 Atmospheric model

Here we define a method to retrieve surface reflectance for the combined (A)ATSR super-pixels given known solar/view geometry and atmospheric constituents, based on approximation of an atmospheric radiative transfer model by look-up tables.

3.4.1 Approximation of atmospheric radiative transfer

For a given sensor waveband, and atmospheric profile, the relationship between surface directional reflectance R_{surf} top of atmosphere reflectance R_{TOA} can be approximated by the equation:

$$R_{TOA}(\theta_v,\theta_s,\phi) = [R_{atm}(\theta_v,\theta_s,\phi) + T(\theta_s)T(\theta_v)\frac{R_{surf}(\theta_v,\theta_s,\phi)}{1-\rho_{atm}R'_{surf}}] \tag{1}$$

where R_{atm} denotes the atmospheric scattering term (TOA reflectance for zero surface reflectance), T denotes atmospheric transmission for either sensor to ground or ground to sensor, and R_{atm} denotes atmospheric bi-hemispherical albedo. The term R'_{surf} denotes ground reflectance for multiple scattered light, and here we use the approximation $R'_{surf} = R_{surf}$.

Table 2: Optical Parameters for four CCI common aerosol models used. Log-normal parameters for two coarse and two fine mode aerosol components and their associated mid-visible refractive indices.

Aerosol component	Refr. index, real part (.55μm)	Refr. Index, imag part (.55μm)	reff (μm)	geom. st dev (σ_i)	variance (ln σ_i)	mode. radius (μm)
Dust	1.56	0.0018	1.94	1.822	0.6	0.788
sea salt	1.4	0	1.94	1.822	0.6	0.788
fine mode weak-abs	1.4	0.003	0.140	1.7	0.53	0.07
fine mode strong-abs	1.5	0.040	0.14	1.7	0.53	0.07

By rearranging (1), the quantity R_{surf} can readily be derived from R_{TOA} by

$$R_{surf}(\theta_v, \theta_s, \phi) = \frac{f}{1 + \rho_{atm} f} \qquad (2)$$

where

$$f = \frac{R_{TOA}(\theta_v, \theta_s, \phi) - R_{atm}(\theta_v, \theta_s, \phi)}{T(\theta_s)T(\theta_v)} \qquad (3)$$

This procedure provides an atmospherically corrected surface directional reflectance (SDR), also referred to as Lambert equivalent reflectance (LER) or bidirectional reflectance factor (BRF). Note that different values of SDR will be retrieved for different view directions.

The calculation is made efficient by pre-compilation of look-up tables for the coefficients defined for each waveband accounting for the spectral response functions Grey et al 2006, using the Vector 6S radiative transfer model (Vermote et al (1997), Kotchenova et al. (2007)), which accounts for polarisation. The model includes Rayleigh scattering, and molecular absorption by the gases O_2, O_3, H_2O, CH_4, N_2O and CO. Although observations at differing view angles will recover a differing surface reflectance value, the surface is approximated as Lambertian for the calculation of multiple scattering terms.

3.4.2 Aerosol model LUT

A set of aerosol models are required to define the optical properties. Pre-compiled LUTs for a set of candidate aerosol models are used to represent a range of aerosol types, based on mixtures of a reduced set of characteristic 'pure' aerosol types. Under Aerosol CCI the four aerosol types chosen to represent these pure aerosol types are two coarse mode aerosol types (sea salt aerosol, desert dust) and two fine mode (weak absorbing, strong absorbing). All assume spherical

particles except for desert dust. Properties are listed in Table 2. Optical properties were calculated using Mie code for the spherical particles, and T-matrix code for desert dust (Dubovik et al., 2006). The properties are fully documented in the *ESA Aerosol_cci Aerosol Model Technical Note*.

These models are used to form 35 mixtures of aerosol types by interpolation of properties (phase function, SSA) according to each 25% fraction within the total aerosol AOD. The Vector 6S code is then used to compute a LUT giving total column atmospheric radiative properties. In operation radiative properties for a continuous distribution of aerosol property variation (coarse/fine ratio, dust fraction etc.) are estimated by tetrahedral interpolation of properties defined at the LUT breakpoints.

Table 3: Aerosol model mixtures used for continuous interpolation

	aerosol components			
model index	coarse mode		fine mode	
	dust	sea-salt	strong-abs	weak-abs
0	0	0	0	100
1	0	0	25	75
2	0	0	50	50
3	0	0	75	25
4	0	0	100	0
5	0	25	0	75
6	0	25	25	50
7	0	25	50	25
8	0	25	75	0
9	0	50	0	50
10	0	50	25	25
11	0	50	50	0
12	0	75	0	25
13	0	75	25	0
14	0	100	0	0
15	25	0	0	75
16	25	0	25	50
17	25	0	50	25
18	25	0	75	0
19	25	25	0	50
20	25	25	25	25
21	25	25	50	0

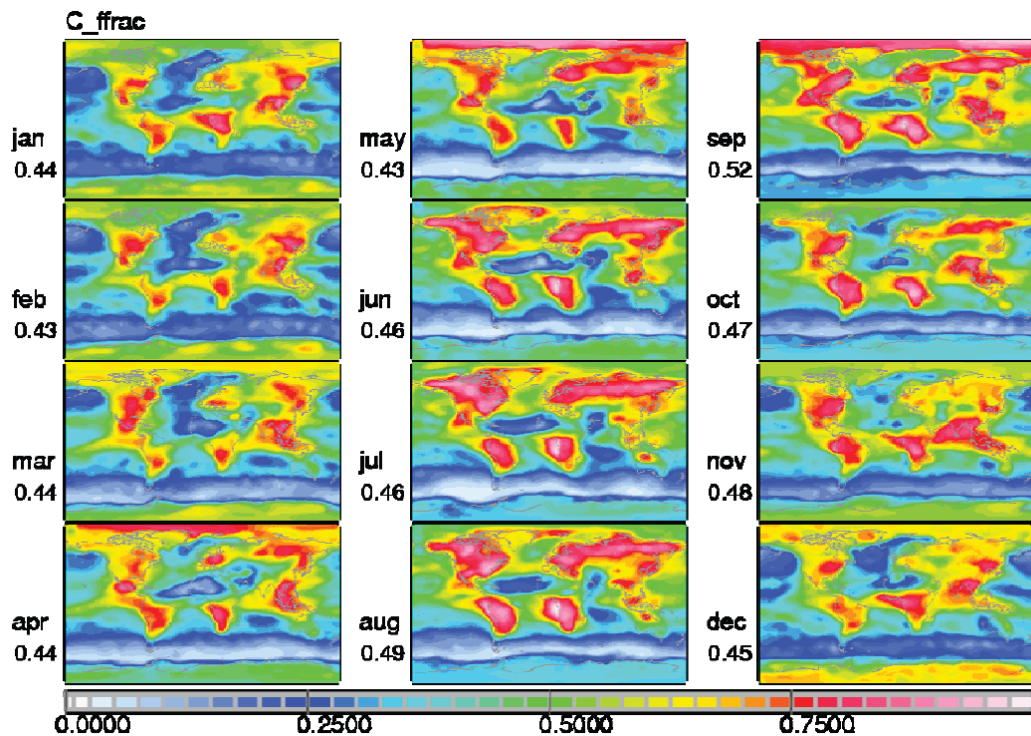|	aerosol components			
model index	coarse mode		fine mode	
	dust	sea-salt	strong-abs	weak-abs
22	25	50	0	25
23	25	50	25	0
24	25	75	0	0
25	50	0	0	50
26	50	0	25	25
27	50	0	50	0
28	50	25	0	25
29	50	25	25	0
30	50	50	0	0
31	75	0	0	25
32	75	0	25	0
33	75	25	0	0
34	100	0	0	0

Figure 2: Example monthly climatology for fine mode fraction of total AOD at 550nm. Similar climatologies are used as input for dust fraction of coarse mode, and weakly absorbing fraction of fine mode AOD.

3.4.3 Aerosol climatology

The climatology of aerosol composition (Kinne et al., 2006) specifies mixing ratios of the four components on a 1° x 1° lat-long grid, separately for each of 12 months, and estimate of AOD. The climatology is derived from merged model median estimates with data from AERONET; an example for fine mode fraction is shown in Figure 2. This is used to provide an *a priori* model of composition for aerosol retrieval, and allowing more robust estimation of properties of aerosol composition and absorption than possible to derive from the imagery alone. In operation, linear interpolation of the following are provided to the retrieval:

(i) Dust fraction of coarse mode AOD (550nm): F_{dust}

(ii) Weakly absorbing fraction of fine mode AOD (550nm): F_{weak}

(iii) Fine mode fraction of total AOD (550nm): FMF

Linear interpolation is used on lat/lon and month to provide an *a priori* estimate of each parameter per retrieval. The first two are used directly and not retrieved. However fine mode fraction of total AOD is used only as a default value – the fine mode AOD in the product is freely retrieved from the data. In addition, over bright desert surfaces, climatology AOD is used a prior estimate in the inversion.

Table 4: Set of break points used for atmospheric look up table (LUT).

Parameter	Range	Interval	Number of breakpoints
RAZ	0 - 180°	20°	20
SZA	0 - 80°	5°	17
VZA			
- *(A)ATSR nadir*	0 - 25°	5°	6
- *(A)ATSR forward*	50-60°	5°	3
AOT (550 nm)	0-2	0.05	41

3.4.4 LUT approximation of RT coefficients

In order to reduce computational cost we use Look Up Tables (LUT) of coefficients calculated by 6S in 4 dimensions. The dimensions are Aerosol Optical Thickness (AOT) at 550nm, relative azimuth angle (RAZ), view zenith angle (VZA) and solar zenith angle (SZA). The tie point set is detailed in Table 4. Each LUT entry contains values for each (A)ATSR waveband of the four coefficients required. In addition for the inversion we require a pre-computed estimate of $D(\theta_s)$ at each waveband, defined as the fraction of total downwelling light at the surface which is diffuse, defined at a fixed surface albedo (0.2). These quantities are pre-computed using the Vector 6S radiative transfer model (Vermote et al 1997; Kotchenova et al., 2007).

A set of LUTs is stored for each aerosol model. During operation we use multidimensional piecewise linear interpolation to obtain the required atmospheric coefficients for given solar/view geometry, waveband and AOT.

From the density of the look-up table grid points and the comparatively smooth behaviour of the TOA reflectance as a function of the LUT dimensions, we can estimate that the error introduced by the LUT approach and the employed linear interpolations is considerably smaller than the expected uncertainties due to selection of aerosol model parameters.

3.4.5 Estimation of surface reflectance

During operation we use multidimensional piecewise linear interpolation to obtain the required atmospheric coefficients (R_{atm}, T, ρ_{atm}, $D(\theta_s)$) for given solar/view geometry, waveband, AOD, aerosol type, and surface pressure. A linear model is applied between neighbouring grid points in all dimensions. This procedure provides an atmospherically corrected surface directional reflectance (SDR), also referred to as Lambertian equivalent reflectance (LER) or bidirectional reflectance factor (BRF). Note that different values of SDR will be retrieved for different view directions.

3.5 Constraints on surface reflectance

To retrieve estimates of aerosol properties from measured satellite radiances, we need to solve the inverse problem to separate the atmospheric and surface scattering contributions to the observed signal. This normally requires some assumptions to be made on the surface reflectance. These assumptions are expressed as constraints defined by error of fit to a parameterized model describing the surface angular or spectral reflectance. Over ocean we use

Table 5: Ocean BRF look-up table – dimensions and breakpoints

Parameter	Range	Interval	Number
SZA			
VZA	same as atmospheric LUT (see Table 4)		
RAZ			
WND-S	1m/s – 21m/s	5m/s	5
WND-D	0° - 270°	90°	4
TAU	0.001 – 3.001	0.1	31
FMF	0 – 1	1	2
BAND	S2, S3, S5, S6		4

a fixed *a priori* model of surface reflectance parameterised by known estimates of wind speed and direction, while over land additional free parameters are fitted to the data for each retrieval.

3.5.1 Ocean surface model

Over ocean, aerosol is retrieved by inversion of either single or dual-angle measurements using a model of ocean surface reflectance. The retrieval is performed where both views are cloud-free and excluding regions of sun glint defined by flags supplied with the AATSR product. A surface model (Koepke, 1984) is used to give an estimate of ocean surface BRDF:

$$\rho_{ocean\_mod} = \rho_{wc} + (1 - f_W)\rho_{gl} + (1 - \rho_{wc})\rho_{sw} \qquad (4)$$

where ρ_{wc} denotes reflectance due to whitecaps , f_W is the fraction of surface covered in whitecaps, ρ_{gl} is the glint reflectance and ρ_{sw} is the water reflectance.

The terms are computed using the models of Cox and Munk (1954) for glint, Monahan & O'Muircheartaigh (1980) and Koepke (1984) for foam fraction and spectral reflectance, and Morel's case I water reflectance model dependent on pigment concentration (Morel 1988). The model is run coupled with the 6SV atmospheric model to account for sky glint. Corresponding values of ocean surface BRF for a range of conditions are precomputed and stored in a LUT. For this computation the ocean pigment concentration is assumed to be a global constant of 0.1 mg/m^{-3}. The ocean BRF will be dependent on the viewing geometry (SZA, VZA, RAZ), wind speed (WND_S) and wind direction (WND_D). The corresponding values are directly available in the L1b product. In addition the LUT will depend on aerosol model (fine mode fraction, FMF) and aerosol optical depth to estimate sky glint. The ocean BRF is provided by the LUT for all spectral bands used for the ocean aerosol retrieval. The 550nm channel is not used due

to high dependence on chlorophyll and sediment. Details on the dimensions and breakpoints of the ocean BRF LUT are presented in Table 5.

3.5.2 Multiple view angle (MVA) constraint over land

We have developed a method for simultaneous estimation of AOD and surface reflectance for data where at least two view angles are available, such as the AATSR and SLSTR (North et al., 1999; North 2002; Grey et al., 2006a,b, Bevan et al., 2012). Methods employing similar principles have also been developed for AATSR and other multi-view sensors, (Veefkind et al., 1999; Diner et al., 2005; Kokhanovsky et al., 2007, Dubovik et al., 2014). The principal advantage of this approach is that no *a priori* information of the surface is required and aerosol properties can be retrieved even over bright surfaces. In the case of multi-view-angle data, a constraint may be made on the angular variation of the land surface reflectance, governed by the BRDF, giving a corresponding error of fit. In particular, the angular variation is assumed to be approximately constant across wavelength, since the angular variation (i.e. shape of the surface bi-directional reflectance distribution) is due principally to geometric effects (e.g. shadowing) which are wavelength independent. This means that for (A)ATSR, the ratio of surface reflectances at the nadir and off-nadir viewing angles (where the view zenith angle is 55°) is well correlated between bands. This avoids the need for assumptions on absolute surface brightness or spectral properties. The method presented here differs from early approaches by using a more sophisticated surface model to account for some spectral variation of the angular shape owing to the variation of the diffuse fraction of light with wavelength.

Scattering of light by atmospheric aerosols tends is be greater at shorter wavelengths. It is important to model the fraction of diffuse to direct radiation since it influences the anisotropy of the surface. The anisotropy is reduced when the diffuse irradiance is high because the contrast between shadowed and sunlit surfaces decreases. Anisotropy is similarly dependent for bright targets owing to the multiple-scattering of light between the surface elements. The atmospheric scattering elements including aerosols and gas molecules are comparable in size to the wavelength of light at optical wavelengths. As a result, the effect of atmospheric scattering on the anisotropy will be a function of wavelength and the shape of the BRDF will vary. Taking these effects into account results is a physical model of spectral change with view angle (North et al., 1999):

$$\rho_{ang\_mod}(\lambda,\Omega) = (1-D(\lambda))v(\Omega)w(\lambda) + \frac{\gamma w(\lambda)}{1-g}\left[D(\lambda) + g(1-D(\lambda))\right] \qquad (5)$$

where $g = 1 - \gamma\omega(\lambda)$, λ is the wavelength, Ω is the viewing geometry (oblique or nadir view), ρ_{ang_mod} is the modelled bidirectional reflectance, γ is the fraction contributing to higher-order scattering and is fixed at 0.35, and D is the fraction of diffuse irradiance. The model separates the angular effects of the surface into two components, a structural parameter v that is dependent only on the viewing and illumination geometry, and the spectral parameter ω, that is dependent only on the wavelength. The free parameters that we need to retrieve through model inversion are $w(\lambda)$ and $v(\Omega)$. Stability was found to be improved by setting $v(\Omega)$ for nadir view to a fixed value of 0.5, and so only the 4 spectral parameters $w(\lambda)$ and oblique view value of $v(\Omega)$ are required to be retrieved.

By inversion of (5), this model of surface scattering has been shown to lead to a tractable method, which is potentially more robust than the simple assumption of angular invariance alone (North 1999). The angular reflectance of a wide variety of natural land surfaces fits this simple model. In contrast, reflectance that is a mixture of atmospheric and surface scattering does not fit this model well. As a result, the model can be used to estimate the degree of atmospheric contamination for a particular set of reflectance measurements and to find the atmospheric parameters which allow retrieval of a realistic surface reflectance.

Next we combine these surface constraints within the scheme of a numerical inversion framework to obtain an optimal estimate of aerosol size and optical depth.

3.6 Numerical inversion

The retrieval algorithm is illustrated in Figure 1. To retrieve the aerosol properties from TOA cloud-free radiances we use a coupled numerical inversion scheme that incorporates the look-up tables derived from the radiative transfer model and a constraint based on a simplified model of land or ocean surface scattering. The basis of the inversion is (i) estimation of surface reflectance (R_{SURF}) for all bands and view angles, for an initial estimate of atmospheric profile, and (ii) iterative refinement of the atmospheric profile to minimise an error metric (E_{mod}) on the surface reflectance set.

3.6.1 AOD retrieval

The input to the algorithm is the TOA reflectance product, averaged over cloud free pixels separately for nadir and oblique views at coarser resolution, referred to as 'superpixel'. The 'superpixel' resolution is at 9km x 9km window for each retrieval. This resolution is appropriate to minimise the effect of errors in image registration, allowing efficient optimisation, while retrieving aerosol within the typical spatial scale of aerosol variability. A set of surface reflectances are calculated for a given atmospheric aerosol model and AOD parameterised by value at 550 nm. An error metric is defined on the surface reflectance set based on a weighted fit to either land or ocean models:

$$E_{\mathrm{mod}} = \sum_{\Omega=1}^{2}\sum_{\lambda=1}^{5} W_{\lambda,\Omega}\left[\rho_{surf}(\lambda,\Omega) - \rho_{ang\_mod}(\lambda,\Omega)\right]^{2} \qquad + \qquad \zeta \qquad (6)$$

$$E_{\mathrm{mod}} = \sum_{\Omega=1}^{2}\sum_{\lambda=2}^{5} W_{\lambda,\Omega}\left[\rho_{surf}(\lambda,\Omega) - \rho_{ocean\_mod}(\lambda,\Omega)\right]^{2} \qquad + \qquad \zeta \qquad (7)$$

where ρ_{ocean_mod} and ρ_{ang_mod} are the surface reflectances estimated using the equations for ocean and land respectively, and ζ is a regularizing function to improve stability. For ρ_{ang_mod} the value is based on the best-fit values of the free parameters. The weight vectors W are defined by estimated uncertainty in observation and model, discussed in Section 3.6.3, where error estimates for retrieved parameters are also given.

For a given atmospheric profile the optimal free parameters of the land surface model that minimize (5) are found through the *Powell* multi-dimensional minimisation routine (Press et al., 1992). For ocean retrieval, the algorithm proceeds with the same inversion framework and aerosol model set as for land but the angular model constraint is simply replaced by a simple metric of fit on the *a priori* ocean reflectance model.

The optimal aerosol properties are found by search for the two parameters (AOD and fine mode fraction) which jointly minimise the estimated error in (6) or (7). Following methods developed in Aerosol CCI, the Brent one-dimensional optimisation method is in two nested iterations: the inner loop to find AOD, and outer loop to find fine mode fraction. The regularizing function ζ is determined by additional constraints discussed below.

3.6.2 Summary of regularizing constraints

A set of practical constraints are included in the inversion to improve stability and impose physical realism on the retrieved model parameters. These provide cost function additions summed to form a value of ζ used in the final cost function minimisation (10).

(i) After TOA -> SDR inversion:

for ocean: check for each channel / view if $\rho_{surf} < -1e\text{-}3$ then $\zeta = \zeta + \rho_{surf}^2 * 1000$

if fmin > 100 skip retrieval

for land: check for each channel / view if $\rho_{surf} < 1e\text{-}3$ then $\zeta = \zeta + (\rho_{surf} - 1e3)^2 * 1000000$

if fmin > 10 skip retrieval

(ii) Limits on the parameters within the land surface model are included within the Powell minimisation, by adding terms to the error fit (E_{mod}) to avoid unrealistic surface reflectance:

if $w(\lambda) < lim (\lambda)$ then $\zeta = \zeta + 1000*(lim (\lambda) - w(\lambda))^2$

where *Iim* = {0.03, 0.02, 0.01, 0.01}

(iii) Constraint on the ratio of forward to nadir parameters. This ratio is compared to the ratio of the TOA reflectance at 1610nm. If the ratio of the surface model parameters exceeds the TOA ratio, then a small penalty cost is added to the fit: $\zeta = \zeta + 10 * \left(\frac{v(Oblique)}{v(Nadir)} - \frac{\rho_{TOA}(1.6, Oblique)}{\rho_{TOA}(1.6, Nadir)} \right)^2$

(iv) A constraint on the curvature of retrieved values of surface reflectance at 550nm - 870 nm is added, which limits over-estimation of AOD over bright non-vegetated surfaces.

The constraint is in the difference between the spectral parameters w(660) and w(550). This is positive only for non-vegetated pixels.

If (w660-w550) > 2 * (w865-w660) then $\zeta = \zeta + 100*((w660-w550) - 2 * (w865-w660))^2$

(v) Constraints on fine mode fitting using Brent:

The following constraints are used for the fitting of the fine mode fraction.

1. To restrict deviation of fine mode fraction from the climatological value, the following is added to the cost returned by Brent: $\zeta = \zeta + 10 * (fot - fot_{clim})^4$. Where fot means the fitted fine mode fraction and fot_{clim} the climatological value.

2. To ensure smoothness a weighted mean of the previously successfully retrieved fine mode values of the previous two lines and two columns (see Table 6) is computed :

$$prevFot = \Sigma(w_i * fot_i) / \Sigma w_i$$
(8)

Where fot_i is the fine mode fraction of the respective pixel and w_i are the weights computed as the inverse quadratic distance:

$$w_i = 1 / ((x_i-x)^2 + (y_i-y)^2) \qquad (9)$$

the following is added to the cost returned by Brent: $\zeta = \zeta + 2* (fot - prevFot)^2$

Initialisation of Brent and setting brackets:

1. Run Brent minimisation with climatology Fine Mode Fraction to determine upper AOD limit

   Use the upper bracket (CX) of this Brent run for all subsequent AOD fits

2. Run Brent for fitting fine mode fraction with limits [0, 1] and starting point at climatology fine mode fraction.

3. Subsequently optimise for each fine mode fraction the AOD using [0, (CX)] as brackets and AOD starting point 0.05

(vi) Constraint on AOD over bright surfaces

Previous versions of the algorithm suggested unstable retrieval in the case of bright surfaces, at high AOD, leading to overestimation of AOD in these cases. Additional constraints are added in this version to stabilize the retrieval in these circumstance.

If the estimated surface NDVI is below 0.5 and the nadir surface reflectance becomes larger than 0.1 at 1.6 um, (NDVI< 0.5 AND ρ_{surf} (1.6) > 0.1):

(vii) Spectral constraint on modelled surface reflectance

To improve stability in the (A)ASTR retrieval, an additional constraint has been included on the variation of surface reflectance. An analogous constraint has been added to the SLSTR retrieval, and follows a similar formulation to the dark target approach used in MODIS (Levy et al., 2007), and the Synergy aerosol retrievals developed for MERIS/AATSR and

SLSTR/OLCI (North et al., 2008; Davies et al., 2015). While these studies used correlation between SWIR and bands located in red and blue regions, but since these wavelength bands are not available to (A)ATSR, and the formulation uses a correlation only between the channels 2 (0.66μm) and 5 (1.6 μm).

The constraint links the surface reflectance terms in the model at the (A)ATSR 1.6 μm and 0.67μm channels, such that we expect $\omega_{0.66}$ to be proportional to $\omega_{1.6}$. Applying the constraint on the surface model parameters rather than reflectance implicitly includes normalization for view angle effects and constrains the information from both view directions.

The constraint is included as a cost function addition given by

$$\zeta = \zeta + \alpha \ (\beta \ \omega_{1.6} - \omega_{0.66})^2$$

where α acts to achieve the optimal relative weighting of this constraint in the inversion, and β describes the ratio between the wavebands. Values for α and β were determined by experiment using aerosol retrievals matched to values from Aeronet sites. Separate pairs of parameters were found for bright/sparsely vegetated surfaces and vegetated surfaces, defined as scenes in the lower and upper quartiles of the NDVI distribution respectively. The addition to the cost function used for any particular scene is determined by linear interpolation based on NDVI of the values calculated using $\alpha = 100.0$, $\beta = 0.5$ at NDVI=0 and $\alpha = 50.0$, $\beta = 0.65$ at NDVI=1.

Table 6: Smoothness constraint weightings. Assuming processing lines first then if the orange is the current pixel, all green pixel cells should already have been processed. Hence these cells are considered for the computation of the previous fine mode fraction.

(x-2/y-2)	(x-1/y)	(x/y-2)	(x+1/y-2)	(x+2/y-2)
(x-2/y-1)	(x-1/y)	(x/y-1)	(x+1/y-1)	(x+2/y-1)
(x-2/y)	(x-1/y)	(x/y)	(x+1/y)	(x+2/y)
(x-2/y+1)	(x-1/y+1)	(x/y+1)	(x+1/y+1)	(x+2/y+1)
(x-2/y+2)	(x-1/y+2)	(x/y+2)	(x+1/y+2)	(x+2/y+2)

Test whether the retrieval AOD becomes larger than the AOD of the Aerocom climatology. If this is the case, the squared difference between retrieved and climatological AOD is added as additional cost to the cost function: $\zeta = \zeta + 0.5 * \Delta \tau^2$

3.6.3 Error propagation and optimization function

Over both land and ocean, the retrieval uses non-linear optimisation of an error function, of the form

$$X^2 = 1/v \sum_{\lambda=1}^{\lambda=4} \sum_{\Omega=0}^{\Omega=1} \frac{(M(\lambda,\Omega) - O(\lambda,\Omega))^2}{\sigma_{M(\lambda,\Omega)}^2 + \sigma_{O(\lambda,\Omega)}^2} \qquad + \quad \zeta \qquad (10)$$

where $\sigma_{M(\lambda,\Omega)}^2$ and $\sigma_{O(\lambda,\Omega)}^2$ denote estimates of 1 s.d. uncertainty in model and observation of surface reflectance at waveband λ and view direction Ω (nadir is here denoted by $\Omega = 0$, oblique view by $\Omega = 1$). The degrees of freedom is denoted by v (independent observations minus free model parameters). It is possible to also include the full covariance matrix into the X^2 formulation, but currently error in model and observations are approximated as uncorrelated between channels.

For a correctly normalised value of chi sq, the estimate of 1 s.d. error in τ_{550} is derived from the second derivative (curvature) of the error surface near the optimal value:

$$\sigma_{\tau 550} = \left(\delta^2 X^2 \Big/ \delta^2 \tau_{550} \right)^{-0.5} \qquad (11)$$

The curvature term is estimated by parabolic fit of the error function for surrounding values of τ_{550}.

The curvature term (a) of the error surface gives a measure of the sensitivity of the location of the minimum to error in model fit. For a steeply curved error surface, the retrieved value of τ_{550} is relatively robust to the estimation of model fit, while for a flat error surface small perturbation in model fit error gives rise to a large error in τ_{550}. For example, over bright surfaces where surface reflectance approaches the 'critical point', where the TOA radiance is insensitive to variation in τ_{550} we have high uncertainty in the derived τ_{550}.

3.6.3.1 Model error over land

Over land, model uncertainty was evaluated by inversion against the test dataset of surface BRDF values computed from a 3D Monte Carlo model. The 3D model and test dataset are described in North (1996) and North et al., (1999). Per channel uncertainties at the four wavebands used were estimated from this and subsequent optimisation:

Over vegetated surface (NDVI>0.7)

$$\sigma_{M\_land} = \{0.01, 0.01, 0.06, 0.02\}$$

Over bright surface (NDVI <0.1):

$$\sigma_{M\_land} = \{0.01, 0.01, 0.02, 0.15\}$$

where the four values listed {0.01…} denote uncertainty at (A)ATSR channels 1-4. For the range 0.1 <=NDVI<=0.7, we use a linear combination of the uncertainties.

3.6.3.2 Model error over ocean

Over ocean the surface model is based on the models of Cox and Munk (1954) for glint, Monahan & O'Muircheartaigh (1980) and Koepke (1984) for foam fraction and spectral reflectance, and Morel's case I water reflectance model. Inputs required *a priori* are surface wind speed W (ms^{-1}) and pigment concentration C (mg m^{-3}).

Uncertainty in ocean reflectance model reflectance is given by sum of the contributions from uncertainty in chlorophyll and wind speed magnitude

$$\sigma^2_{M\_ocean\_W} = \sigma^2_{M\_ocean\_W} + \sigma^2_{M\_ocean\_C} \tag{12}$$

Where

$$\sigma_{M\_ocean\_W} = \left| M\_ocean(\lambda, \Omega, W + \sigma_W, C) - M\_ocean(\lambda, \Omega, W + \sigma_W, C) \right| \tag{13}$$

$$\sigma_{M\_ocean\_W} = \left| M\_ocean(\lambda, \Omega, W, C + \sigma_C) - M\_ocean(\lambda, \Omega, W + \sigma_W, C) \right| \tag{14}$$

Uncertainties in wind speed and pigment concentration are assigned values of 3 ms^{-1} and 0.1 mg m^{-3} respectively.

3.6.3.3 Observation errors

The per-channel observation error gives an estimate of the 1 s.d. uncertainty in derived land surface reflectance, and includes errors due to instrument calibration, radiative transfer model and LUT, and uncertainty in aerosol absorption parameterization.

$$\sigma^2_O = \sigma^2_{RT} + \sigma^2_{inst} + \sigma^2_{AerMod} \tag{15}$$

Approximations for these are given by:

$$\sigma^2_{inst} = T_S(\lambda, \theta)(a_\lambda + b_\lambda R_{TOA}(\lambda, \theta)), \tag{16}$$

The figures for (A)ATSR used are:

a={0.0005, 0.0003, 0.0003, 0.0003 }

b={0.024, 0.032, 0.02, 0.033 }

Where the four values listed in brackets denote uncertainty at (A)ATSR channels 1-4. In practice the *b* term is only implemented, *a* is neglected.

The term *Ts* gives scaling from TOA to surface at

$$T_S(\lambda,\Omega) = \frac{\delta R_{SURF}(\lambda,\Omega)}{\delta R_{TOA}(\lambda,\Omega)}$$

(17)

and is derived from the LUT coefficients at time of inversion.

Based on Kotchenova and Vermote (2007), error due to RT at all channels is approximated as

$$\sigma_{RT}^2 = 0.006$$

(18)

The error due to uncertainty in aerosol absorption is approximated by

$$\sigma_{AerMod} = 0.05 R_{atm}(\lambda,\Omega)$$

(19)

where R_{atm} denotes atmospheric path reflectance, estimated from LUT values.

3.6.3.4 Practical implementation of cost function error estimate

Once the optimal AOD and fine mode fraction are determined successfully the uncertainty needs to be computed as described above. The estimation of AOD uncertainty requires the curvature of the cost function at the optimal AOD. The curvature corresponds to the second partial derivate of the cost function wrt to AOD. Since the second derivate is not available analytically it will be approximated assuming a parabolic behaviour of the cost function around the minimum. To fit the parabola three points are required. The first is the minimum, i.e. the optimal AOD with the associated cost. Additionally two points need to be computed. Ideally the additional two points should be close to the minimum and bracket the minimum on both sides. However, the choice of these points needs to consider the following aspects:

- The points should be always inside the AOD range of the LUT.

- Due to computational limits, the cost function is not necessarily smooth on small intervals of AOD, especially if the cost function is relatively flat. This requires the choice of points sufficiently apart from the minimum.

- In cases of dark surface the optimal AOD may account for almost all reflectance signal in some channels. In these cases the retrieval is forced to avoid producing negative surface reflectance by a smooth penalty function for higher AOD. This penalty function leads to a steep increase of the cost function not related to the actual uncertainty of the AOD. To safely avoid this kind of situation points will be chosen for AOD smaller than the optimal AOD.

In general the cost is computed on $\{0.7*\tau_{opt}, 0.85*\tau_{opt}, \tau_{opt}\}$ with τ_{opt} being the retrieved AOD at minimal cost. One exception is made for $\tau_{opt} < 0.05$ when the lowest point is set to 0.002 instead of $0.7*\tau_{opt}$.

As the exact performance of the algorithm and thus the estimation of uncertainty will depend on the actual S3 data it may be required to adjust the absolute range of uncertainties by a scaling factor which will only be determined in the validation phase, after processing actual data. It is however of advantage to prepare for the possibility of a constant scaling factor for land and ocean respectively.

Furthermore uncertainties over land should ultimately have a lower limit of $0.02+0.05*\tau_{opt}$. Over ocean a minimum value of 0.02 for uncertainty should be used.

In the case where the curvature of the cost function is not positive, the corresponding quality flag should be raised and $0.02+0.05*\tau_{opt}$ is to be used as default value for uncertainty.

3.7 Post-processing

The detection of cloud can be very challenging and perfect screening of cloud, especially optically thin clouds, is nearly impossible. However, even a very small or thin cloud can have strong impacts on the AOD retrieval. In the case of cloud contamination the AOD reported will be unreasonably high. The fact that clouds have a much larger spatial variability compared to typical aerosol distributions can be exploited to implement a post-processing step (Sogacheva et al., 2017).

The processing is a subsequent step after AOD retrieval has successfully finished for a larger region. It is a simple image processing considering all neighbours of a retrieved superpixel, i.e. boxes of 9 (3x3) superpixels. For an individual AOD retrieval to pass successfully this step of filtering the following criteria need to be met:

- at least 3 neighbouring superpixels with successful retrievals are required

- the sample corrected standard deviation of the valid superpixels in the 3x3 box needs to be smaller than 0.1

$$\sigma_\tau = \sqrt{\left(\frac{1}{N_{valid}-1}\sum_1^{N_{valid}}(\tau_i - \overline{\tau_i})^2\right)} < 0.1 \qquad (20)$$

3.8 Derivation of further aerosol outputs

The optimal aerosol model is selected by search for the two parameters (AOD and fine mode fraction) which jointly minimise the cost function (10). Further parameters are derived from these using stored information on the aerosol components:

As previously described the retrieval of AOD and fine mode fraction relies on the assumptions made on the optical properties of the aerosol. To allow a simple retrieval to cover a wide range of the naturally occurring variation only 4 basic aerosol components are mixed continuously based on retrieval cost of the fit (for fine mode fraction) or based on a climatological distribution to predetermine the amount of absorption in the fine mode or dust in the coarse mode. Ultimately the retrieved AOD will be the best fitting result based on these assumptions.

To enable understanding about the retrieval but also to provide more associated information to the retrieval for more detailed subsequent analysis of the AOD product additional derived product information on the assumed aerosol properties is provided.

The following list will provide the respective equations, how these derived products are computed:

- **Spectral AOD**

  Only AOD at 550nm is directly provided by the fit process. In order to derive the associated AODs at other wavelengths a look-up table is provided which gives the ratio $r_{550,\lambda}$ between AOD_λ at other instrument wavelengths and AOD_{550} for any of the 35 pre-computed aerosol mixtures. On interpolation between the 35 mixtures during the retrieval process these ratios need to be interpolated accordingly. Hence any other spectral AOD is computed using these interpolated ratios:

$$AOD_\lambda = r_{550,\lambda}\, AOD_{550} \tag{21}$$

  Respective uncertainties are calculated assuming the same proportional error as for AOD550.

- **Angstrøm exponent α**

  The wavelength dependence of AOD can be approximated by a power law relation. The exponent **α** of this power law approximation can be computed based on a pair of spectral AOD values. Here we choose 865nm and 550nm.

$$\frac{AOD_{865}}{AOD_{550}} = \left(\frac{865nm}{550nm}\right)^{-\alpha} \tag{22}$$

  Using the previous relation for spectral AOD this yields:

$$\alpha = \frac{\ln\left(r_{550,865}\right)}{\ln(550)-\ln(865)} \tag{23}$$

- **Single scattering albedo**

   Single scattering albedo (SSA) values are provided in the look-up table for each of the 35 mixtures and for each of the wavelength. Similar to the ratios of spectral AOD these need to be interpolated to the retrieved mixture. The output simply is the interpolated value for each wavelength.

- **Absorbing AOD**

   Absorbing AOD (AAOD) represents the total amount of absorption by the given aerosol mixture. It is therefore directly based on SSA. The AAOD at 550nm is computed by:

$$AAOD = (1 - SSA)AOD_{550} \tag{24}$$

- **Dust AOD**

   Dust AOD (D_AOD) represents the aerosol optical depth of the dust particles in the respective aerosol mixture. With the fine mode fraction and the fraction of dust in the coarse mode the dust AOD is computed as:

$$D_{AOD} = (1 - f_{FM})f_{DUST}AOD_{550} \tag{25}$$

- **Spectral surface reflectance**

   The provided spectral surface directional reflectances (SDR) are the averaged SDRs on super-pixel resolution resulting from atmospheric correction using the retrieved aerosol properties and optical depth.

4 OUTPUTS AND DATA FORMAT

4.1 AOD and related aerosol parameters

The algorithm output is the estimated AOD and best fitting aerosol model for each successful retrieval. The algorithm also outputs the uncertainty in AOD at 550nm., and surface reflectance at all solar reflective channels. Further aerosol optical properties, such as Angstrom, are derived based on those of the returned aerosol model. The image grid of retrieved AOD products is resampled for L2 output to a 10km sinusoidal grid, stored in NetCDF 4 as a one dimensional vector. In addition, the algorithm performs a L3 monthly composite at 1 deg of aerosol AOD, modal aerosol type and surface reflectance. The output is summarised in Table 7.

Table 7: Level 2 stripline products

Level 2 (stripline) products	Waveband	Spatial resolution
AOD for best-fit model	550 nm	10 km
Error (1 s.d.) in AOD	550 nm	
AAOD	550 nm	
AOD	659 nm	
Error (1 s.d.) in AOD		
AOD	865 nm	
Error (1 s.d.) in AOD		
AOD	1610 nm	
Error (1 s.d.) in AOD		
D_AOD	550 nm	
FM_AOD	550 nm	
Angstrom	550/865 nm	
SSA	550 nm	
Best-fit model properties: Ratio Coarse/fine (retrieved) Ratio Dust/sea salt (clim.) Ratio Weak/strong abs (clim)	550 nm	10 km
Nadir surface reflectance	550, 670, 870 and 1600 nm	1-10 km
	550, 670, 870 and 1600 nm	1-10 km
Applied cloud mask		1-10 km
Latitude		
Longitude		
Pixel corner latitude 1..4		
Pixel corner longitude 1...4		
Sun_zenith		
Satellite_zenith		
Relative azimuth		
Time		
Land sea flag		

5 PRACTICAL CONSIDERATIONS FOR IMPLEMENTATION

The algorithm is implemented in C. The code is modular, and uses pre compiled LUTs which may be readily changed to allow an arbitrary set of aerosol models. Timing shows a single daylight orbit typcially requires 20mins execution on a single processor 2.6Ghz Linux workstation. The code has been implemented at Swansea University on a Linux cluster with high number of cores (~400) to allow global processing of 1 year in ~48 hours. The code is also implemented at the UK Jasmin facility allowing direct access to (A)ATSR archive at UK PAC. Code verification has taken place between implementations by testing retrievals on a fixed dataset, and validation globally by automated comparison of AOT output with all available AERONET stations.

6 CONCLUSIONS

This report summarises the SU-ATSR algorithm Version 4.35, for retrieval of aerosol properties from the ATSR and AATSR instruments. Over land, the algorithm uses the AATSR dual-view capability to estimate aerosol without prior assumptions of land surface spectral properties. Over ocean the algorithm uses the low spectral reflectivity at red, near and mid infra-red channels to constrain aerosol retrieval using a priori estimates of wind speed and chlorophyll concentration. An analytic estimate of error in AOD is also made. In addition to AOD, we retrieve we retrieve aerosol fine mode fraction, and corresponding aerosol model which gives an estimate of further aerosol properties. The data are produced both coincident with satellite overpass (Level 2) and as monthly composites (Level 3) at 0.1° resolution. Successful retrievals are possible over all regions, including bright desert surfaces, but excluding areas of sun glint, snow or cloud.

Limitations of the algorithm are that (i) it will perform retrieval only over snow, ice and glint-free surfaces, (ii) at least 50% of pixels within the 9km super-pixel must be free of cloud, (iii) the algorithm should not be run for solar angles > 70°. Retrieval is of higher quality over darker surfaces, such as dense vegetation and ocean, whereas for bright desert surfaces the relatively weaker aerosol signal makes the retrieval more uncertain. For (A)TSR, the sampling geometry generally leads to greater accuracy over land in the Northern hemisphere, where aerosol forward scattering is sampled by the oblique view. While there are not additional quality flags, the uncertainty due to geometry and surface brightness are captured within the per-retrieval uncertainty estimate.

REFERENCES

AERONET. Available online: http://aeronet.gsfc.nasa.gov/ (accessed on 22 March 2020).

Aerosol_cci Project. Available online: http://www.esa-aerosol-cci.org/ (accessed on 22 March 2021).

Aguirre, M., B. Berruti, J-L. Bezy, M. Drinkwater, F. Heliere, U. Klein, C. Mavrocordatos, P. Silvestrin, B. Greco, J. Benveniste, (2007) Sentinel-3 The Ocean and Medium-Resolution Land Mission for GMES Operational Services, *ESA Bulletin* **131**, 24-29.

Alton, P.B., North, P. R. J. and Los, S. O. (2007). The impact of diffuse sunlight on canopy light-use efficiency, gross photosynthetic product and net ecosystem exchange in three forest biomes, *Global Change Biology*, **13(4)**, doi:10.1111/j.1365-2486.2006.01316.x.

Barton, I. J., Zavody, A. M., O'Brien, D. M., Cutten, D. R., Saunders, R. W., & Llewellyn-Jones, D.T. (1989). Theoretical algorithms for satellite-derived sea-surface temperatures. *Journal of Geophysical Research - Oceans*, **94**, 3365 – 3375.

Bellouin, N., O. Boucher, J. Haywood, and M.S. Reddy, (2005): Global estimation of aerosol direct radiative forcing from satellite measurements, *Science*, **438**, 1138-1141.

Berthelot, B. and Dedieu, G., Operational method to correct VEGETATION satellite measurements from atmospheric effects. Proceedings IGARSS 2000. *IEEE 2000 International*. 01/02/200002/2000; 2:831-833 vol.2. DOI: 10.1109/IGARSS.2000.861718.

Bevan, S.L., North, P.R.J., Grey, W.M.F., Los, S.O. and Plummer, S.E. (2009), Impact of atmospheric aerosol from biomass burning on Amazon dry-season drought. *Journal of Geophysical Research*, **114**, D09204, doi:10.1029/2008JD011112.

Bevan, S.L., North, P.R.J., Los, S.O. and Grey, W.M.F. (2012). A global dataset of atmospheric aerosol optical depth and surface reflectance from AATSR. *Remote Sensing of Environment*, **116**, 119-210.

Cox, C. and Munk, W. (1954) Measurements of the roughness of the sea surface from photographs of the Sun's glitter. J. Opt. Soc. Am., 44, 838–850.

Davies, W.H., North, P.R.J., Grey, W.M.F. and Barnsley, M.J. (2010), Improvements in Aerosol Optical Depth Estimation using Multi-angle CHRIS/PROBA Images, *IEEE Transactions on Geoscience and Remote Sensing,* **48**(1), 18-24.

Davies, W. & North, P. (2015). Synergistic angular and spectral estimation of aerosol properties using CHRIS/PROBA-1 and simulated Sentinel-3 data. *Atmospheric Measurement Techniques* 8(4), 1719-1731.

de Leeuw, G., Holzer-Popp, T., Bevan, S., Davies, W., Descloitres, J., Grainger, R. G., Griesfeller, J., Heckel, A., Kinne, S., Klüser, L., Kolmonen, P., Litvinov, P., Martynenko, D., North, P. J. R., Ovigneur, B., Pascal, N., Poulsen, C., Ramon, D., Schulz, M., Siddans, R., Sogacheva, L., Tanré, D., Thomas, G. E., Virtanen, T. H., von Hoyningen Huene, W., Vountas, M., & Pinnock, S., Evaluation of seven European aerosol optical depth retrieval algorithms for climate analysis, *Remote Sensing of Environment*, **2015**, *162*, 295 -315.

Diner, D. J., Asner, G. P., Davies, R., Knyazikhin, Y., Muller, J. P., Nolin, A. W., Pinty, B., Schaaf, C. B., & Stroeve, J. (1999). New directions in Earth observing: scientific applications of multiangle remote sensing. Bulletin of the American Meteorological Society, **80** (11), 2209 – 2228.

Diner, D., J. Martonchik, R. Kahn, B. Pinty, N. Gobron, D. Nelson, and B. Holben, (2005). Using angular and spectral shape similarity constraints to improve MISR aerosol and surface retrievals over land, *Remote Sensing of Environment*, **94**, 155-171.

Dubovik, O., (2005). Optimization of Numerical Inversion in Photopolarimetric Remote Sensing, in *Photopolarimetry in Remote Sensing, NATO Science Series II: Mathematics, Physics and Chemistry*, Springer Netherlands, ISBN 978-1-4020-2368-2 (Online), 65-106.

Dubovik, O., Sinyuk, A., Lapyonok, T., Holben, B.N., Mishchenko, M., Yang, P., Eck, T.F., Volten, H.,Munoz, O., Veihelmann, B. et al. (2006) Application of light scattering by spheroids for accounting for particle non-sphericity in remote sensing of desert dust. J. Geophys. Res., 111.

Dubovik, O. Lapyonok, T. Litvinov, P. Herman, M. Fuertes, D. Ducos, F. Lopatin, A., Chaikovsky, A.,Torres, B., Derimian, Y. et al. (2014). GRASP: A versatile algorithm for characterizing the atmosphere. *Proc. SPIE 2014*.

Fell F. and J. Fischer, (2001). Numerical simulation of the light field in the atmosphere-ocean system using the matrix-operator method, *JQSRT*, **69**, 351-388.

Fischer, J. and Grassl, H. (1984). Radiative transfer in an atmosphere-ocean system: an azimuthally dependent matrix-operator approach, *Appl. Optics* **23**, 1035-1039.

Fischer and Preusker (2009), Radiative Transfer Model Description Document for ESA AATSR/MERIS Synergy project, available online at http://www.brockmann-consult.de/beam-wiki/display/SYN/Documents.

Flowerdew, R. J., & Haigh, J. D. (1996). Retrieval of aerosol optical thickness over land using the ATSR-2 dual look radiometer. *Geophysical Research Letters*, **23** (4), 351 – 354.

Govaerts, Y. M., S. Wagner, A. Lattanzio, and P. Watts (2010), Joint retrieval of surface reflectance and aerosol optical depth from MSG/SEVIRI observations with an optimal estimation approach: 1. Theory, *J. Geophys. Res.*, **115**, D02203, doi:10.1029/2009JD011779.

Grey., W.M.F., North., P.R.J., Los, S.O., and Mitchell, R.M., (2006). Aerosol optical depth and land surface reflectance from multi-angle AATSR measurements: Global validation and inter-sensor comparisons. *IEEE Transactions on Geoscience and Remote Sensing,* **44(8)**, 2184 – 2197.

Grey., W.M.F, North., P.R.J., and Los, S. (2006b). Computationally efficient method for retrieving aerosol optical depth from ATSR-2 and AATSR data, *App. Optics*, **45(12):** 2786-2795.

Guanter, L.; M. Del Carmen González-Sanpedro, J. Moreno, (2007), A method for the atmospheric correction of ENVISAT/MERIS data over land targets, *International Journal of Remote Sensing*, **28(3-4),** 709-728.

Hess, M., P. Koepke, and I. Schult, 1998: Optical Properties of Aerosols and Clouds: The Software Package OPAC. *Bull. Amer. Meteor. Soc.,* **79**, 831–844.

Holben, B., et al. (2001) An emerging ground-based aerosol climatology: Aerosol optical depth from AERONET, J. Geophys. Res., 106(D11), 12067-12097.

Holzer-Popp, T., Schroedter, M. and Gesell, G. (1999). High-Resolution Aerosol Maps Exploiting the Synergy of ATSR-2 and GOME , *Earth Observation Quarterly* (65): 19-24, ESA Publications Division, ISSN 0256 - 596X.

Holzer-Popp, T., M. Schroedter-Homscheidt, H. Breitkreuz, L. Klüser, D. Martynenko, (2008). Synergetic aerosol retrieval from SCIAMACHY and AATSR onboard ENVISAT, *Atmospheric Chemistry and Physics Discussions*, **8**, 1-49.

Holzer-Popp, T., de Leeuw, G., Griesfeller, J., Martynenko, D., Klüser, L., Bevan, S., Davies, W., Ducos, F., Deuzé, J. L., Graigner, R. G., Heckel, A., von Hoyningen-Hüne, W., Kolmonen, P., Litvinov, P., North, P., Poulsen, C. A., Ramon, D., Siddans, R.,

Sogacheva, L., Tanre, D., Thomas, G. E., Vountas, M., Descloitres, J., Griesfeller, J., Kinne, S., Schulz, M., & Pinnock, S., Aerosol retrieval experiments in

Hsu, N. C., S.-C. Tsay, M. D. King, and J. R. Herman, (2004) Aerosol properties over bright-reflecting source regions, *IEEE Transactions on Geoscience and Remote Sensing*, **42**(3), 557– 569.

Hsu, N. C. ,. Jeong, M.-J, Bettenhausen, C.,. Sayer, A. M, Hansell, R., Seftor, C. S. , Huang, J. and Tsay, S.-C. (2013). Enhanced Deep Blue aerosol retrieval algorithm: The second generation. *Journal of Geophysical Research*, **118**, 1–20, doi:10.1002/jgrd.50712, 2013

IPCC. Climate Change 2013: The Physical Science Basis; Contribution of Working Group I to the Fifth Assessment Report of the Intergovernmental Panel on Climate Change; Stocker, T.F., Qin, D., Plattner, G.-K., Tignor, M.,Allen, S.K., Boschung, J., Nauels, A., Xia, Y., Bex, V., Midgley, P.M., Eds.; Cambridge University Press: Cambridge, UK; New York, NY, USA, 2013; p. 1535.

Jacquemoud, S., & Baret, F. (1990). PROSPECT: a model of leaf optical properties spectra, *Remote Sensing of Environment*, **34**, 75-9.

Jeong, M.-J., and N. C. Hsu (2008), Retrievals of aerosol single-scattering albedo and effective aerosol layer height for biomass-burning smoke: Synergy derived from "A-Train" sensors, *Geophys. Res. Lett.*, **35**, L24801, doi:10.1029/2008GL036279.

Kaufman Y. J. and Sendra, C. (1988). Algorithm for automatic corrections to visible and near IR satellite imagery, *Int. J. Remote Sensing*, **9**, 1357-1381.

Kaufman, Y.J. and Tanré D. (1992), Atmospherically resistant vegetation index (ARVI) for EOS-MODIS, *IEEE Transactions on Geoscience and Remote Sensing*, **30**, 261-270.

Kinne et al., (2006). An AeroCom initial assessment – optical properties in aerosol component modules of global models, *ACP*, **6**, 1-22, 2006.

Koepke, P. (1984). Effective Reflectance of Oceanic Whitecaps, *Applied Optics*, 23(11), 1816-1824.

Kokhanovsky, A.A., F.-M. Breon, A. Cacciari, E. Carboni, D. Diner, W. Di Nicolantonio, R.G. Grainger, W.M.F.Grey, R. Holler, K.-H. Lee, P.R.J. North, A. Sayer, G. Thomas, W. von Hoyningen-Huene, (2007). Aerosol remote sensing over land: satellite retrievals using different algorithms and instruments. *Atmospheric Research,* **85**, 372-394, doi:10.1016/j.atmosres.2007.02.008.

Kolmonen, P., Sogacheva, L., Virtanen, T.H., de Leeuw, G., Kulmala, M. (2015). The ADV/ASV AATSR aerosol retrieval algorithm: Current status and presentation of a full-mission AOD data set. Int. J. Digit. Earth.

Kotchenova, S.Y., Vermote, E.F., Matarrese, R. and Klemm, F.J. (2006), Validation of a vector version of the 6S radiative transfer code for atmospheric correction of satellite data. Part I: path radiance. *Applied Optics*. 10/2006; **45**(26):6762-74.

Leroy M., Deuze J.L., Bréon F.M., Hautecoeur O., Herman M., Buriez J.C., Tanre D., Bouffies S., Chazette P., and Roujean J.L., (1997). Retrieval of atmospheric properties and surface bidirectional reflectances over the land from POLDER. *Journal of Geophysical Research* **102** (D14), 17023-17037.

Levy, R.C., Remer, L., Mattoo, S., Vermote, E. and Kaufman, Y.J. (2007), Second-generation algorithm for retrieving aerosol properties over land from MODIS spectral reflectance. *J. Geophys. Res.*, **112**, D13211, doi:10.1029/2006JD007811.

Levy, R.C.; Munchak, L.A.; Mattoo, S.; Patadia, F.; Remer, L.A.; Holz, R.E. Towards a long-term global aerosol optical depth record: Applying a consistent aerosol retrieval algorithm to MODIS and VIIRS-observed reflectance. Atmos. Meas. Tech. **2015**, 8, 4083–4110.

Lyapustin, A. and Wang, Y., (2009). The time series technique for aerosol retrievals over land from MODIS, in Satellite Aerosol Remote Sensing Over Land, A. A. Kokhanovsky and G. DeLeeuw, Eds. Heidelberg: Springer Praxis Books, ISBN: 978-3-540-69396-3, pp. 69–99.

Mackay, G., M.D. Stevens, and J.A. Clark (1998). An atmospheric correction procedure for the ATSR-2 visible and near-infrared land surface data. *Int. J. Remote Sensing* **19**, 2949-2968.

Martonchik, J.V., D.J. Diner, R. A. Kahn, T.P. Ackerman, M. M. Verstraete, B. Pinty, and H.R. Gordon,(1998). Techniques for retrieval of aerosol properties over land and ocean using multiangle imagery. *IEEE Trans. Geosci. Rem. Sens.* **36**, 1212-1227

McGill, M.J., L. Li, W.D. Hart, G.M. Heymsfield, D.L. Hlavka, P.E. Racette, L. Tian, M.A. Vaughan, and D.M. Winker, (2004). Combined lidar-radar remote sensing: initial results from CRYSTAL-FACE, *Journal of Geophysical Research*, 109, doi: 10.1029/2003JD004030.

Mishchenko M.I., I.V. Geogdzhayev, B. Cairns, B.M. Carlson, J. Chowdhary, A.A. Lacis, L. Liu, W.B. Rossow, L.D. Travis, (2007). Past, present, and future of global aerosol climatologies derived from satellite observations: A perspective, Journal Of Quantitative Spectroscopy & Radiative Transfer **106 (1-3)**, 325-347.

Monahan, E.C. and O'Muircheartaigh, I. (1980). Optimal power-law description of oceanic whitecap dependence on wind speed, *Journal of Physical Oceanography*, **10**(12), 2094–2099, 1980.

North, P.R.J. (1996), Three-dimensional forest light interaction model using a Monte Carlo method, *IEEE Transactions on Geoscience and Remote Sensing*, **34(5)**, 946-956.

North, P.R.J., Briggs, S.A., Plummer, S.E. and Settle, J.J., (1999). Retrieval of land surface bidirectional reflectance and aerosol opacity from ATSR-2 multi-angle imagery, *IEEE Transactions on Geoscience and Remote Sensing*, **37(1),** 526-537.

North, P.R.J. (2002a). Estimation of fAPAR, LAI and vegetation fractional cover from ATSR-2 imagery. *Remote Sensing of Environment* **80**:114–121.

North, P. R. J. (2002b). Estimation of aerosol opacity and land surface bidirectional reflectance from ATSR-2 dual-angle imagery: Operational method and validation, *J. Geophys. Res.*, **107**, doi:10.1029/2000JD000,207.

North, P.R.J., Brockmann , C., Fischer, J., Gomez-Chova, L., Grey, W., Hecklel A., Moreno, J., Preusker, R. and Regner, P. (2008). MERIS/AATSR synergy algorithms for cloud screening, aerosol retrieval and atmospheric correction. *In Proc. 2nd MERIS/AATSR User Workshop, ESRIN, Frascati, 22- 26 September 2008.* (CD-ROM), ESA SP-666, ESA Publications Division, European Space Agency, Noordwijk, The Netherlands.

Press, W.H., S.A. Teukolsky, W.T. Vetterling, and B.P. Flannery, (1992). N*umerical Recipes in C, The Art of Scientific Computing (Second Edition).* Cambridge: Cambridge University Press.

Prieto-Blanco, A., North, P.R.J., Fox, N. and Barnsley, M.J. (2009). Satellite-driven modelling of Net Primary Productivity (NPP): Theoretical analysis. *Remote Sensing of Environment* **113(1),** 137-14.

Rahman, H., and G. Dedieu (1994). SMAC : A simplified method for the atmospheric correction of satellite measurements in the solar spectrum. *International Journal of Remote Sensing*, **15**(1), 123-143.

Rathke, C and Fischer, J, (2002). Efficient parameterization of the infrared effective beam emissivity of semitransparent atmospheric layers, *J. Geophys. Res.,* **107** (D4), doi:10.1029/2001JD000596.

Remer, L. Y. Kaufman, D. Tanre, S. Mattoo, D. Chu, J. Martins, R.-R. Li, C. Ichoku, R. Levy, R. Kleidman, T. Eck, E. Vermote, and B. Holben, (2005). The MODIS Aerosol Algorithm, Products and Validation, *Journal of the Atmospheric Sciences*, **62**, 947-973.

Rosenfeld, D., Y. Rudich, R. Lahav, (2001). Desert dust suppressing precipitation: A possible desertification feedback loop, *Proceedings of the National Academy of Sciences*, **98**, 11, 5975-5980, doi:10.1073/pnas.101122798.

Saint, G., (1994). "VEGETATION" onboard SPOT 4, Products Specifications, Version 2, 18 May 1994.

Santer, R., V. Carrère, P. Dubuisson and J.C. Roger (1999), Atmospheric corrections over land for MERIS, *Int. J. Remote Sensing*, **20** (9), 1819-1840.

Santer, R., D. Ramon, J. Vidot, E. Dilligeard, (2007). A surface reflectance model for aerosol remote sensing over land, *International Journal of Remote Sensing*, **28(3-4)**, 737-760.

Santer, R. (2009): MERIS L2 ATBD 2.15, http://envisat.esa.int/instruments/meris/atbd/atbd_2_15.pdf

Smirnov, A., Holben, B.N., Slutsker, I., Giles, D.M., McClain, C.R., Eck, T., Sakerin, S.M., Macke, A., Croot, P., Zibordi, G., et al. (2009). Maritime Aerosol Network as a component of Aerosol Robotic Network. J. Geophys. Res., 114.

Smith, D., Poulsen, C. and Latter, B (2008), Calibration Status of AATSR and MERIS Reflectance Channels, *In Proc. 2nd MERIS/AATSR User Workshop, ESRIN, Frascati*, *22-26 September 2008*. (CD-ROM), ESA SP-666, ESA Publications Division, European Space Agency, Noordwijk, The Netherlands.

Solomon , S., et al., (2007). "Technical Summary: The Physical Science Basis. Contribution of Working Group I to the Fourth Assessment Report of the Intergovernmental Panel on Climate Change," in Climate Change 2007, S. Solomon, D. Qin, M. Manning, Z. Chen, M. Marquis, K. B. Averyt , M. Tignor, and H. L. Miller, Eds. Cambridge, United Kingdom and New York, NY, USA: Cambridge University Press.

Thomas, G.E., E. Carboni, A.M. Sayer, C.A. Poulsen, R. Siddans, R.G. Grainger (2009), Oxford-RAL Aerosol and Cloud (ORAC): aerosol retrievals from satellite radiometers, in Satellite Aerosol Remote Sensing Over Land, A. A. Kokhanovsky and G. de Leeuw (eds.), Springer, 2009.

Twomey, S.A. (1974). Pollution and the planetary albedo, *Atmospheric Environment*,. **8,** 1251–56.

Veefkind, J. P., de Leeuw, G., Durkee, P. A., Russell, P. B., Hobbs, P. V., & Livingston, J. M. (1999). Aerosol optical depth retrieval using ATSR-2 and AVHRR data during TARFOX. *Journal of Geophysical Research - Atmospheres*, **104** (D2), 2253 – 2260.

Veefkind J.P., G. de Leeuw, P. Stammes , R.B.A. Koelemeijer, (2000). Regional distribution of aerosol over land, derived from ATSR-2 and GOME, *Remote Sensing of Environment*, **74** (3), 377-386.

Vermote E.F., D. Tanré , J.L. Deuze, M. Herman, J.J. Morcrette, (1997): Second Simulation of the Satellite Signal in the Solar Spectrum, 6S: An overview, *IEEE Transactions on Geoscience and Remote Sensing,* **35(3),** 675-686.

Vidot, J., Santer, R., and Aznay, O. (2008) Evaluation of the MERIS aerosol product over land with AERONET, Atmos. Chem. Phys., 8, 7603-7617.

von Hoyningen-Huene W., Freitag M., and Burrows, J.B. (2003), Retrieval of aerosol optical thickness over land surfaces from top-of-atmosphere radiance, *Journal of Geophysical Research*, **108 (D9):** Art. No. 4260.

von Hoyningen-Huene, W. et al. (2006). Simultaneous determination of aerosol and surface characteristics from top-of-atmosphere reflectance using MERIS on board of Envisat, *Advances in Space Research*, **37**, 2172-2177.

Von Hoyningen-Huene, W., et al.: IBAER ATBD, http://www.brockmann-consult.de/beam/software/plugins/baer-1.0.0/BAER_ATBD_NOV-3160-NT-2703_v2.0.pdf

End of the document